

# Theory of chiral edge state lasing in a two-dimensional topological system

Matteo Seclì,<sup>1,\*</sup> Massimo Capone,<sup>1,2</sup> and Iacopo Carusotto<sup>3,†</sup>

<sup>1</sup>*International School for Advanced Studies (SISSA), Via Bonomea 265, I-34136 Trieste, Italy*

<sup>2</sup>*CNR-IOM Democritos, Via Bonomea 265, I-34136 Trieste, Italy*

<sup>3</sup>*INO-CNR BEC Center and Dipartimento di Fisica, Università di Trento, I-38123 Povo, Italy*

(Dated: December 20, 2024)

We theoretically study topological laser operation in a bosonic Harper-Hofstadter model featuring a saturable optical gain. Crucial consequences of the chirality of the lasing edge modes are highlighted, such as an ultraslow relaxation time even well above threshold and a sharp dependence of the lasing threshold on the geometrical shape of the amplifying region. In between the convective and the absolute (lasing) thresholds, a strong amplification of a propagating probe beam is found. Our results provide the starting point for a theory of the coherence properties of topological lasers.

PACS numbers: 03.65.Vf, 42.60.Da, 42.65.Sf, 73.43.-f

Starting with the pioneering observation of topologically protected chiral edge modes around a time-reversal-breaking two-dimensional photonic crystal [1, 2], the last decade has witnessed the explosion of the field of *topological photonics*. Taking inspiration from condensed matter physics concepts such as topological insulators and quantum Hall effects, new exciting optical effects were found, which are now opening the way to technological applications [3, 4].

So far, experiments have mostly addressed single-particle topological features, which are observable via the linear optical properties of the system: besides the direct evidences of the topological order such as chiral edge states in different geometries, dimensionalities, platforms, and spectral regions [2, 5–9], remarkable results were the measurement of the band Berry curvature [10], the observation of magnetic Landau levels [11], of topological pumping [12], of anomalous Floquet edge states [13, 14], of synthetic dimensions [15, 16]. Beyond linear optics, a great attention is nowadays being devoted to the rich interplay between optical nonlinearities and topology: nonlinearity-driven topological phase transitions [17] and self-localized states [18] were anticipated for classical light, while the strongly correlated quantum Hall states of light predicted for ultra-strong nonlinearities [5, 19, 20] have recently started being experimentally investigated in circuit-QED platforms [21].

One of the most promising applications of topological photonics concerns laser operation in topological systems displaying optical gain, the so-called *topological lasing*. As a first step, lasing into the zero-dimensional edge states of a one-dimensional Su-Schrieffer-Heeger (SSH) chain was proposed [22] and experimentally demonstrated [23–25]. Soon afterwards, lasing into the one-dimensional chiral edge states of a two-dimensional topological lattice was experimentally realized in suitably designed semiconductor laser devices [26, 27]. Such devices appear promising to solve a long-standing technological problem in opto-electronics, namely the realization of large-area devices for high-power coherent emission [28]:

a pioneering theoretical work [29] has in fact pointed out that the topological protection against fabrication defects should make laser operation into topological edge states to remain single mode and to have a high slope efficiency even well above the laser threshold. This optimistic view was somehow questioned in [30] for the specific case of semiconductor-based devices: using a standard model of laser operation in these systems, dynamical instabilities stemming from the combination of nonlinear frequency shifts and of the slow carrier relaxation time were predicted, in close analogy to what is observed in polariton lasers [31].

The purpose of this Letter is to build a generic theory of topological laser operation and isolate those features that directly stem from the chirality of the lasing mode and thus differentiate topological lasers from standard ones. To avoid getting lost in effects that are specific to some classes of devices only, our strategy will be to keep the model complexity at a minimum level and focus on the basic effects. This will provide powerful conceptual tools for future studies of the complex nonlinear physics of specific devices and, on a longer run, of the fundamental quantum limits of topological laser operation.

*The model* – As the topological origin of our predictions guarantees their general applicability to a wide class of models, in this work we will concentrate on the most celebrated bosonic Harper-Hofstadter (HH) model [3]. Modulo the extra pseudo-spin associated to the propagation direction around the ring cavities [5, 32], this model underlies the topological laser operation of [27]. In the Landau gauge, the HH Hamiltonian reads [33]:

$$H = \sum_{m,n} \left\{ \omega_0 a_{m,n}^\dagger a_{m,n} - J (a_{m,n}^\dagger a_{m+1,n} + e^{-i2\pi\vartheta m} a_{m,n}^\dagger a_{m,n+1} + \text{h.c.}) \right\}, \quad (1)$$

where the sum runs over all the sites of the lattice,  $\omega_0$  is the natural frequency of the microrings, and  $a_{m,n}$  is the photon field amplitude at the site  $(m, n)$ . In the chosen gauge, the hopping amplitude along the  $x$  direc-

tion is real and constant and equal to  $J$ , while hopping along  $y$  involves a  $x$ -dependent phase. The strength of the synthetic magnetic field is quantified by the flux  $\vartheta$  per plaquette in units of the magnetic flux quantum. For rational  $\vartheta = p/q$ , the bulk eigenstates distribute in  $q$  bands. In spatially finite systems, chiral edge states unidirectionally propagating around the system appear in the energy gaps between the bands. In what follows we will focus on the simple  $\vartheta = 1/4$  case, whose dispersion of band and edge states is sketched in Fig.1(a).

Making use of the semiclassical theory of lasing under the assumption that the gain medium instantaneously responds to the field [34], losses and gain can be included as additional terms in the time-evolution of the classical field amplitudes  $a_{m,n}$  [29, 35],

$$\dot{a}_{m,n}(t) = -i [a_{m,n}, H] + \left( \frac{P_{m,n}}{1 + \beta |a_{m,n}|^2} - \gamma \right) a_{m,n}. \quad (2)$$

Here  $\gamma$  is the intrinsic loss coefficient of the resonators,  $P_{m,n}$  determines the spatial profile of the gain, and the  $\beta$  coefficient sets the gain saturation level. This is the simplest model that is able to include the band topology and to describe laser operation, so it perfectly serves our purpose of isolating the general features of topological lasing. The numerical results discussed in the following are obtained by simulating the dynamical evolution (2) until a steady-state is found. A small Gaussian noise is added to the zero-field initial state  $a_{m,n} = 0$  to trigger the laser oscillation process.

*Whole system gain (WSG)* – We start our investigation from the case of a finite ( $25 \times 25$ ) lattice with a spatially uniform  $P_{m,n} = P$  gain. Fig.1(c) shows how the lasing threshold remains very close to the single-resonator value  $P_0 \doteq \gamma$  analytically extracted from (2), the laser emission is spread throughout the whole system, and the slope efficiency  $d|a|^2/dP$  is only slightly lower than the single-site value. Due to the complex mode competition between the different sites, no monochromatically oscillating steady state is reached and the strong spatio-temporal modulation persists indefinitely [Fig.1(b)]. Such chaotic behaviours are very commonly found in laser arrays unless some specific stabilization scheme is introduced [28, 36–38], and our results do not suggest any specific signature of the non-trivial topology of the HH bands. An example of time evolution is illustrated in the Supplemental Video 1.

*Whole edge gain (WEG)* – A natural strategy to favor laser emission in the topological edge states over the bulk ones is to restrict the gain to the sites on the geometrical border of the system. This scheme was experimentally implemented in [27] [39]. In agreement with earlier theoretical work [29], Fig.1(b) displays a stable monochromatic single mode oscillation on the system edge. Both the threshold and the slope efficiency shown by the blue curve in Fig.1(c) are very close to the single-site ones. The slight increase in the threshold to  $\tilde{P}_0 \gtrsim P_0$

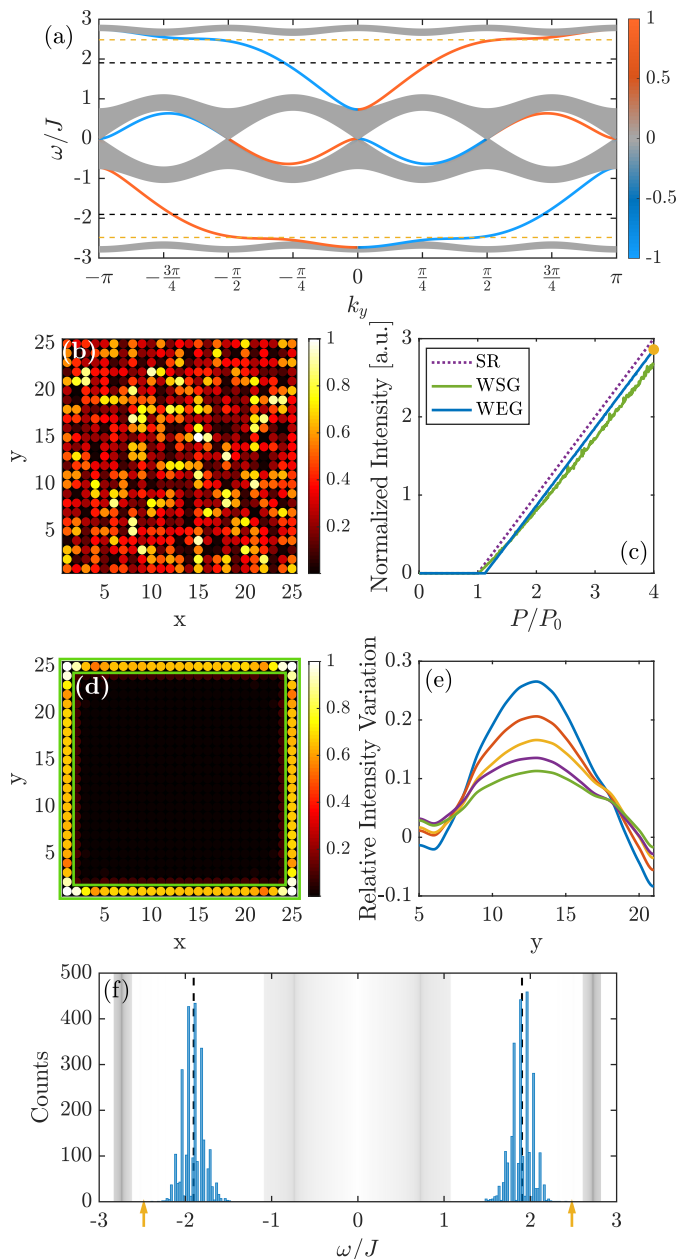


Figure 1. Top panel (a): energy bands of the conservative Harper-Hofstadter Hamiltonian (1) with flux  $\vartheta = 1/4$  in a lattice of  $N_x = 399$  sites along  $x$  and periodic boundary conditions along  $y$ . Blue vs. red color scale quantifies localization on the left or right edges. The horizontal black and orange lines indicate the WEG and PEG lasing frequencies shown in (f). Panels (b-f): Topological lasing in a  $25 \times 25$  HH lattice with  $\vartheta = 1/4$ . Panel (b): snapshot of the (normalized) intensity distribution at  $t = 1000/\gamma$  for WSG. Panel (c): spatially averaged intensity (normalized to the number of amplifying sites) vs. gain strength. Panel (d): snapshot of the (normalized) steady-state intensity distribution for a one-site-thick WEG. The green rectangle indicates the amplifying sites. Panel (e): cuts of the intensity distribution along the  $x = 1$  line at times (from top to bottom)  $\gamma t = 4385, 5165, 5945, 6720, 7500$ . Panel (f): probability distribution of the lasing frequency for WEG. The dashed lines indicate the center of mass of the distribution, the orange arrows indicate the lasing frequency for a  $1 \times 15$  PEG. The gray shading indicates the density of states of the bands in (a).

is mostly due to the weak but finite penetration of the edge mode into the lossy bulk. The topological nature of the lasing mode is witnessed by the value of the oscillation frequency, which is located in a gap of the band structure [Fig.1(a,f)], as well as by the robustness of the single-mode emission against a weak disorder on the site frequencies (not shown). Since the gain is broadband, oscillation occurs with the same probability in either gap. In contrast, the dynamical instabilities found in [30] were due to specific features of semiconductor lasers, in particular the presence of a slow carrier reservoir that induces site-dependent nonlinear frequency shifts.

While these results recover previous theoretical investigations [29], some additional features emerge under a closer look. Fig.1(f), for instance, shows that the lasing frequency is randomly chosen within relatively broad distributions. As usual in ring lasers, the mode spacing is fixed by the round-trip quantization  $\Delta\omega \simeq 2\pi v_g/L$  where  $v_g$  is the group velocity of the edge mode and  $L$  is the perimeter of the system. While the  $k$ -dependent spatial overlap of the edge modes with the gain region makes the effective gain to be frequency-dependent and peaked roughly at the center of the gap, the details of the mode selection process crucially depend on the initial noisy seed at each instance of lasing. Once the lasing mode is selected, the single-mode emission remains then stable indefinitely.

As an even more remarkable feature, Fig.1(e) displays a series of longitudinal cuts of the intensity profile along the  $x = 1$  left edge for different times separated by an (approximate) round-trip time  $T_{rt} = L/v_g$ . The intensity modulation due to the initially noisy state relaxes away on a much slower time-scale than all other microscopic scales, including  $T_{rt}$ . As an illustrative example, Supplemental Video 2 shows an intensity bump traveling in the clockwise direction around the system and slowly fading away. In a follow-up work, this ultra-slow relaxation rate will be analytically explained within the general theory of the collective modes of a laser device [40] in terms of the weakly frequency-dependent effective gain and of the weak dispersion of the edge mode.

*Partial edge gain (PEG)* – Since this ultra-slow relaxation is likely to compromise the coherence of the emission under the effect of quantum noise, it is interesting to explore topological laser operation in a different configuration where the gain is restricted to a finite strip of sites along an edge. Since the chiral motion at  $v_g$  forces any perturbation to be quickly expelled from the amplifying region, one can reasonably expect that relaxation will be dramatically faster in this case. At the same time, the absence of topologically protected winding numbers [41] in this geometry allows the mode profile to continuously relax towards its optimal shape.

This physics is illustrated in Fig.2. As expected, a steady-state with a stable monochromatic oscillation is quickly reached on a characteristic timescale set by the

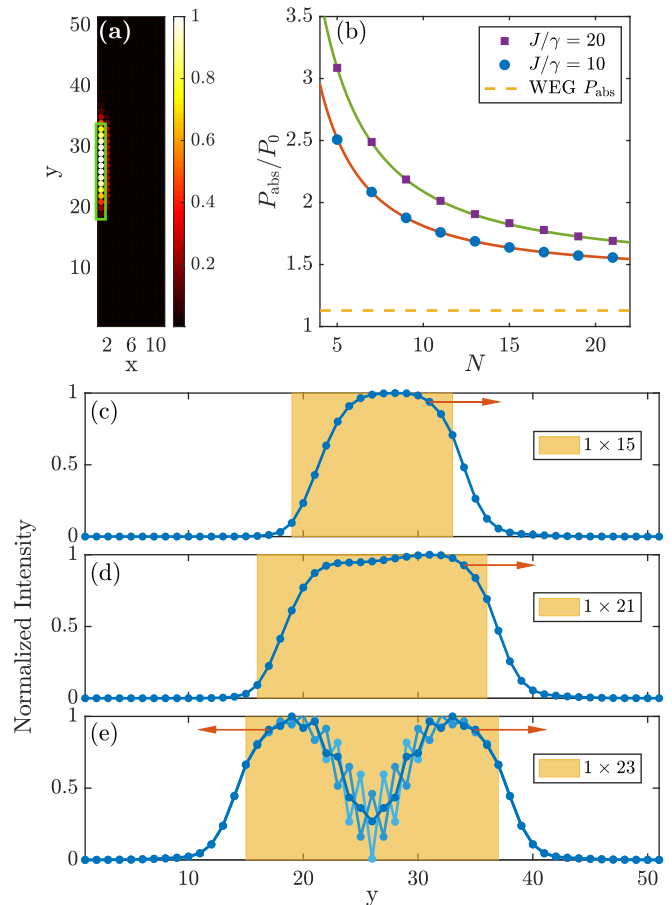


Figure 2. Panel (a): steady-state intensity distribution for a  $1 \times 15$  PEG. The green rectangle indicates the amplifying sites located on the edge of a much larger  $11 \times 51$  lattice. Panel (b): lasing threshold for  $1 \times N$  PEG with different  $J/\gamma = 20, 10$  (solid lines). Lasing threshold for a one-site-thick WEG case (dashed line). Panels (c-e): cuts of the intensity distribution along the  $x = 1$  line for different PEG geometries (see legends). The shaded area indicates the amplifying sites. The curves in (c,d) refer to the steady-state; the different curves in (e) refer to different times separated by  $0.05\gamma^{-1}$ .

microscopic scales of the system. As previously, laser operation is equally likely to take place into the edge modes located in either of the energy gaps and displaying opposite chiralities. For moderate values of  $N$  [panels (c) and (d)], mode competition is able to efficiently funnel all the emission into a single edge mode, randomly chosen at each realization. The chosen chirality then controls the direction along which emission extends from the amplifying sites into the neighboring ones, e.g. in the upwards direction in panel (a). The situation is very different for large values of  $N$ . In this case, mode competition is not able to isolate a single mode and lasing simultaneously occurs in modes of both chiralities, as shown in panel (e). Nonetheless, local gain saturation effects are still able to keep the two chiralities spatially separated with a net outward flow (red arrows). Given the large frequency

difference (of order  $J$ , and visible as a fast temporal beating in the small central overlap region) between the two modes, single-mode emission can be recovered just by using a weakly frequency-dependent gain medium [42].

*Convective vs. absolute instability* – Additional intriguing features of the PEG case are found in the dependence of the lasing threshold on the strip length  $N$  plotted in Fig.2(b). As expected the threshold is found to decrease for growing  $N$ , but a numerical fit of the form  $aN^{-b}+c$  clearly shows that the large- $N$  limit remains significantly higher than the WEG threshold (dashed line).

An explanation for this remarkable finding is offered by the distinction between convective and absolute instabilities, a well-known phenomenon in the theory of non-linear dynamical systems and in hydrodynamics [43–45]. The *absolute instability* (AI) threshold  $P_{\text{abs}}$  corresponds to the standard dynamical instability of the zero-field state. The *convective instability* (CI) is instead a weaker form of instability that is found whenever the exponential growth of a perturbation for  $P > \tilde{P}_0$  is overcompensated by its quick motion at  $v_g$ : in this CI regime, even though the *peak* amplitude of the moving perturbation grows in time, its *local* value at any given spatial location quickly decreases back to zero. When the amplifying region is spatially finite as in our PEG case, any perturbation immediately disappears upon entering the external lossy region. This distinction between CI and AI explains why the laser instability is only observed above the higher AI threshold  $P_{\text{abs}} > \tilde{P}_0 \gtrsim P_0$ . Of course this phenomenon does not occur in the WEG case where the closed shape of the amplifying region does not allow the perturbation to escape from it.

A key quantitative signature of this physics is the dependence of the absolute threshold on the group velocity  $v_g$ , a quantity that in our model is directly controlled by  $J$ . To validate our interpretation, we have thus repeated the calculation of the threshold for a higher value of  $J/\gamma$ : while the WEG threshold at  $\tilde{P}_0 \gtrsim P_0$  does not change [dashed line in Fig.2(b)], the PEG one at  $P_{\text{abs}}$  monotonically grows with  $J$  [squares vs. circles] confirming the role of  $v_g$ . A further evidence in this direction is found in the value of the lasing frequency above threshold: in the WEG case, the group velocity plays no role so that maximization of the spatial overlap with gain favours lasing around the gap centers [Fig.1(f)]. In the PEG case, instead, the location of the absolute threshold  $P_{\text{abs}}$  is dominantly controlled by  $v_g$ , so the AI is first reached by slow edge modes located next to the outer edge of the gaps (orange arrows).

The possibility of an efficient traveling-wave amplification [46] in the CI regime is illustrated in Fig.3. We consider a system of  $11 \times 25$  sites with amplification restricted to a  $1 \times 7$  vertical strip located on the left border and extending from site 10 to site 16. The chiral transmission of a coherent probe through the gain region is studied using a pair of input and output waveguides cou-

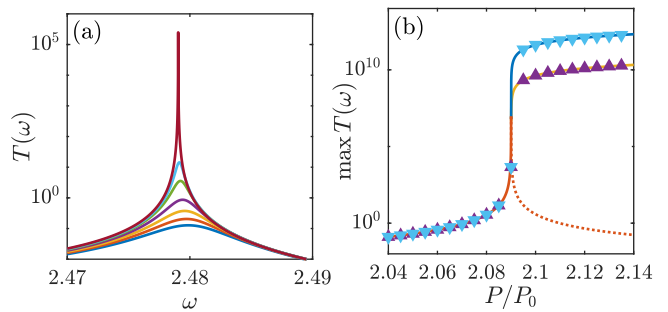


Figure 3. Left panel (a): Incident-frequency-dependent transmission spectrum for different gain strengths (from bottom to top)  $P/P_0 = 2.04, 2.05, 2.06, 2.07, 2.08, 2.085, 2.09$  approaching the lasing threshold for a  $1 \times 7$  PEG. Right panel (b): peak transmittivity as a function of gain strength for incident amplitude  $E_0/\sqrt{J} = 10^{-7}$  (upwards triangles) or  $10^{-8}$  (downwards triangles). Red lines indicate the result of the linearized calculation.

pled to the neighboring sites 8 and 18 on the same border. The transmission is calculated by solving the temporal evolution until the steady state is reached. As usual in input-output theory [47], new terms must be added to the equations of motion for the input and output sites,

$$\dot{a}_{\text{in}}(t) = \dots - \frac{\gamma_{\text{in}}}{2} a_{\text{in}} - \sqrt{\gamma_{\text{in}}} E_0 e^{-i\omega t} \quad (3)$$

$$\dot{a}_{\text{out}}(t) = \dots - \frac{\gamma_{\text{out}}}{2} a_{\text{out}} \quad (4)$$

where the dots  $\dots$  summarize the RHS of (2), the incident field has amplitude  $E_0$  and frequency  $\omega$ , and  $\gamma_{\text{in,out}}$  account for the extra losses due to the waveguides; the transmittivity is then obtained from the transmitted field  $E_{\text{out}} = \sqrt{\gamma_{\text{out}}} a_{\text{out}}$  as  $T = |E_{\text{out}}/E_0|^2$ . The results are shown in Fig.3. Below the lasing threshold  $P_{\text{abs}}$ , the full numerical calculations (triangles) are perfectly recovered by a simpler linearized calculation based on the Green’s function approach for a weak probe (red lines), as discussed in the SM of [32] and further developed at the quantum level in [46]. Above the threshold, the linearized calculations are of course no longer reliable as nonlinear effects dominate the physics.

Panel (a) shows the transmission spectrum for gain values in the CI region  $\tilde{P}_0 < P < P_{\text{abs}}$ . For  $P < P_0$ , gain is not able to overcome losses: the net absorption of all sites combined with the impedance mismatch at the input and output waveguides conspire to give a very low transmission. As  $P$  grows above  $\tilde{P}_0$ , net amplification sets in, giving a broad transmission peak. As  $P$  further grows towards  $P_{\text{abs}}$ , the transmittivity grows far above 1 in a narrow frequency range and eventually diverges at the lasing frequency as the absolute threshold is approached ( $P \rightarrow P_{\text{abs}}^-$ ). Panel (b) shows the peak transmittivity as a function of gain strength for two values of the probe intensity. Well below the laser threshold, the two curves coincide as the system behaves in a linear way.

Around and above threshold, instead, nonlinear gain saturation sets in, limiting the effective amplification. Well above the laser threshold, the field intensity is fixed by the self-oscillation process independently of the probe, so the transmittivity is inversely proportional to  $|E_0|^2$ .

*Conclusions* – In this Letter, we have reported a theoretical study of a topological laser device based on a bosonic Harper-Hofstadter lattice model displaying optical gain. Focusing our attention on laser operation into a topologically protected edge mode, we have highlighted the striking consequences of the chirality of the lasing mode: when gain is distributed around the whole edge, lasing can occur in a number of closely-spaced modes and relaxation towards the steady-state occurs on a very slow timescale; when gain is restricted to a finite strip, the distinction between convective and absolute instabilities causes an increase of the threshold and introduces new amplification regimes. The generality of our theory provides the conceptual building blocks to describe a wide class of specific topological laser devices and, on a longer run, for the development of a quantum theory of the ultimate coherence properties of topological lasers.

Continuous exchanges with M. Wouters on the subject of convective and absolute instabilities are warmly acknowledged. We are grateful to T. Ozawa and H. M. Price for stimulating discussions. I.C. acknowledges funding from Provincia Autonoma di Trento. M.C. acknowledges support from MIUR PRIN 2015 (Prot. 2015C5SEJJ001) and SISSA/CNR project “Superconductivity, Ferroelectricity and Magnetism in bad metals” (Prot. 232/2015).

---

\* [matteo.secli@sisssa.it](mailto:matteo.secli@sisssa.it)

† [iacopo.carusotto@unitn.it](mailto:iacopo.carusotto@unitn.it)

- [1] F. D. M. Haldane and S. Raghu, *Physical Review Letters* **100**, 013904 (2008).
- [2] Z. Wang, Y. D. Chong, J. D. Joannopoulos, and M. Soljačić, *Nature* **461**, 772 (2009).
- [3] T. Ozawa, H. M. Price, A. Amo, N. Goldman, M. Hafezi, L. Lu, M. C. Rechtsman, D. Schuster, J. Simon, O. Zilberberg, and I. Carusotto, arXiv preprint (2018), [arXiv:1802.04173](https://arxiv.org/abs/1802.04173).
- [4] L. Lu, J. D. Joannopoulos, and M. Soljačić, *Nature Photonics* **8**, 821 (2014).
- [5] M. Hafezi, S. Mittal, J. Fan, A. Migdall, and J. M. Taylor, *Nature Photonics* **7**, 1001 (2013).
- [6] M. C. Rechtsman, J. M. Zeuner, Y. Plotnik, Y. Lumer, D. Podolsky, F. Dreisow, S. Nolte, M. Segev, and A. Szameit, *Nature* **496**, 196 (2013).
- [7] T. Jacqmin, I. Carusotto, I. Sagnes, M. Abbarchi, D. D. Solnyshkov, G. Malpuech, E. Galopin, A. Lemaître, J. Bloch, and A. Amo, *Physical Review Letters* **112**, 116402 (2014).
- [8] J. Ningyuan, C. Owens, A. Sommer, D. Schuster, and J. Simon, *Physical Review X* **5**, 021031 (2015).
- [9] L. Lu, Z. Wang, D. Ye, L. Ran, L. Fu, J. D. Joannopoulos, and M. Soljačić, *Science* **349**, 622 (2015).
- [10] M. Wimmer, H. M. Price, I. Carusotto, and U. Peschel, *Nature Physics* **13**, 545 (2017).
- [11] N. Schine, A. Ryou, A. Gromov, A. Sommer, and J. Simon, *Nature* **534**, 671 (2016).
- [12] Y. E. Kraus, Y. Lahini, Z. Ringel, M. Verbin, and O. Zilberberg, *Physical Review Letters* **109**, 106402 (2012).
- [13] S. Mukherjee, A. Spracklen, M. Valiente, E. Andersson, P. Öhberg, N. Goldman, and R. R. Thomson, *Nature Communications* **8**, 13918 (2017).
- [14] L. J. Maczewsky, J. M. Zeuner, S. Nolte, and A. Szameit, *Nature Communications* **8**, 13756 (2017).
- [15] E. Lustig, S. Weimann, Y. Plotnik, Y. Lumer, M. A. Bandres, A. Szameit, and M. Segev, arXiv preprint (2018), [arXiv:1807.01983](https://arxiv.org/abs/1807.01983).
- [16] O. Zilberberg, S. Huang, J. Guglielmon, M. Wang, K. P. Chen, Y. E. Kraus, and M. C. Rechtsman, *Nature* **553**, 59 (2018).
- [17] D. Leykam and Y. D. Chong, *Physical Review Letters* **117**, 143901 (2016).
- [18] Y. Lumer, Y. Plotnik, M. C. Rechtsman, and M. Segev, *Physical Review Letters* **111**, 243905 (2013).
- [19] J. Cho, D. G. Angelakis, and S. Bose, *Physical Review Letters* **101**, 246809 (2008).
- [20] R. O. Umucalılar and I. Carusotto, *Physical Review Letters* **108**, 206809 (2012).
- [21] P. Roushan, C. Neill, A. Megrant, Y. Chen, R. Babush, R. Barends, B. Campbell, Z. Chen, B. Chiaro, A. Dunsworth, A. Fowler, E. Jeffrey, J. Kelly, E. Lucero, J. Mutus, P. J. J. O’Malley, M. Neeley, C. Quintana, D. Sank, A. Vainsencher, J. Wenner, T. White, E. Kapit, H. Neven, and J. Martinis, *Nature Physics* **13**, 146 (2017).
- [22] L. Pillozzi and C. Conti, *Physical Review B* **93**, 195317 (2016).
- [23] P. St-Jean, V. Goblot, E. Galopin, A. Lemaître, T. Ozawa, L. Le Gratiet, I. Sagnes, J. Bloch, and A. Amo, *Nature Photonics* **11**, 651 (2017).
- [24] M. Parto, S. Wittek, H. Hodaei, G. Harari, M. A. Bandres, J. Ren, M. C. Rechtsman, M. Segev, D. N. Christodoulides, and M. Khajavikhan, *Physical Review Letters* **120**, 113901 (2018).
- [25] H. Zhao, P. Miao, M. H. Teimourpour, S. Malzard, R. El-Ganainy, H. Schomerus, and L. Feng, *Nature Communications* **9**, 981 (2018).
- [26] B. Bahari, A. Ndao, F. Vallini, A. El Amili, Y. Fainman, and B. Kanté, *Science* **358**, 636 (2017).
- [27] M. A. Bandres, S. Wittek, G. Harari, M. Parto, J. Ren, M. Segev, D. N. Christodoulides, and M. Khajavikhan, *Science* **4005**, 1 (2018).
- [28] S. Longhi and L. Feng, *APL Photonics* **3**, 060802 (2018).
- [29] G. Harari, M. A. Bandres, Y. Lumer, M. C. Rechtsman, Y. D. Chong, M. Khajavikhan, D. N. Christodoulides, and M. Segev, *Science* **4003**, 1 (2018).
- [30] S. Longhi, Y. Kominis, and V. Kovanis, *Europhysics Letters* **122**, 14004 (2018).
- [31] F. Baboux, D. De Bernardis, V. Goblot, V. N. Gladilin, C. Gomez, E. Galopin, L. Le Gratiet, A. Lemaître, I. Sagnes, I. Carusotto, M. Wouters, A. Amo, and J. Bloch, *Optica* **5**, 1163 (2018).
- [32] M. Hafezi, E. A. Demler, M. D. Lukin, and J. M. Taylor, *Nature Physics* **7**, 907 (2011).
- [33] D. R. Hofstadter, *Physical Review B* **14**, 2239 (1976).

- [34] M. O. Scully and M. S. Zubairy, *Quantum Optics* (Cambridge University Press, 1997) pp. xvi, 630.
- [35] M. Seclì, *Edge State Lasing in a 2D Topological Photonic System*, [Msc thesis](#), University of Trento, Trento (2017).
- [36] H. G. Winful and S.-S. Wang, [Applied Physics Letters](#) **53**, 1894 (1988).
- [37] A. Hohl, A. Gavrielides, T. Erneux, and V. Kovanic, [Physical Review Letters](#) **78**, 4745 (1997).
- [38] J. Katz, S. Margalit, and A. Yariv, [Applied Physics Letters](#) **42**, 554 (1983).
- [39] Note that topological lasing in [26] was operated under a WSG. The physical reason why bulk mode lasing was suppressed in this experiment is presently under investigation.
- [40] M. Wouters and I. Carusotto, [Physical Review Letters](#) **99**, 140402 (2007).
- [41] N. D. Mermin, [Reviews of Modern Physics](#) **51**, 591 (1979).
- [42] Note that the pseudo-spin degree of freedom in [27] allows for more complex field configurations where modes of both chiralities are excited even in a monochromatic steady-state. As discussed there, more complex ring-resonators are then required to favour one chirality.
- [43] M. C. Cross and P. C. Hohenberg, [Reviews of Modern Physics](#) **65**, 851 (1993).
- [44] R. J. Deissler, [Journal of Statistical Physics](#) **40**, 371 (1985).
- [45] M. Santagiustina, P. Colet, M. San Miguel, and D. Walgraef, [Physical Review Letters](#) **79**, 3633 (1997).
- [46] V. Peano, M. Houde, F. Marquardt, and A. A. Clerk, [Physical Review X](#) **6**, 041026 (2016).
- [47] C. W. Gardiner and M. J. Collett, [Physical Review A](#) **31**, 3761 (1985).